Aerodynamic Force Calculations of an Elliptical Circulation Control Airfoil

M. Sun,* S. I. Pai,† and I. Chopra‡
University of Maryland, College Park, Maryland

A method is developed to predict the aerodynamic forces on a circulation control elliptical airfoil in a two-dimensional flow environment. By distributing source panels on the airfoil surface in the separation region and using conformal mapping techniques, a simple solution for the potential flow including effects of separated wake is obtained. The development of boundary layers and wall-jet is calculated by a finite difference method. The potential flow with separated wake effect calculations and boundary layer and wall-jet calculations are combined in an iterative process to determine the aerodynamic forces under given jet momentum coefficient and freestream condition. The effect of separated wake is found significant for a cylinder. The correlation of the calculation results with the available experimental data appears reasonable.

Nomenclature

a = semimajor axis of an ellipse
b = semiminor axis of an ellipse
c = airfoil chord length
C_s = source strength
C_L = lift coefficient, based on airfoil chord length
C_p = static pressure coefficient
C_μ = blowing momentum coefficient, $J/\frac{1}{2}\rho U_\infty^2 c$
f = nondimensional stream function
h_1, h_2 = matrical coefficients in elliptical coordinate, x_e, y_e
J = blowing momentum flux per span
N = number of source panels
P = static pressure
P_0 = total pressure
$\bar{P}$ = nondimension static pressure, $(P-P_0)/(\rho U_\infty^2)$
q_j = source panel strength
r, θ = polar coordinates
R = radius
Re = Reynolds number, based on airfoil chord length, $(U_\infty c)/v$
S_U, S_L = separation points of upper and lower boundary layer
U_∞ = freestream speed
U, V = x-directional and y-direction mean flow velocity
U', V' = x-direction and y-direction fluctuation velocity
U_e = flow speed at boundary layer edge
$W(z)$ = complex potential function
x_c, y_c = Cartesian coordinate system
x_e, y_e = elliptical coordinate system
$\tilde{x}, \tilde{y}$ = transformed coordinate system
y_{eo} = coordinate line along elliptical airfoil surface
Z = complex variable, $x_c + iy_c$
α = angle of attack
γ = nondimensional circulation
Γ = circulation
ϵ = eddy-viscosity
ζ = complex variable, $\xi + i\eta$
λ = ratio, b/a
v = kinematic viscosity
ξ, η = Cartesian coordinate system
ρ = mass density
ϕ = velocity potential function
ψ = stream function

Subscripts

c = circular
C = Cartesian
s = source
e = elliptical

Received Jan. 16, 1985; revision received Feb. 6, 1985.

*Postdoctoral Fellow, Center for Rotorcraft Education and Research, Department of Aerospace Engineering.
†Professor Emeritus, Institute for Physical Science and Technology.
‡Professor, Center for Rotorcraft Education and Research, Department of Aerospace Engineering.

Introduction

In a circulation control airfoil, a thin jet of air is blown from a spanwise slot along a rounded trailing edge (Fig. 1). The air jet remains attached over the curved surface because of the Coanda effect (the balance of centrifugal force and suction pressure). This results in an increase in the circulation around the airfoil. The circulation generated can be easily controlled by altering the momentum of the blowing jet. The circulation control airfoil can achieve a high lift coefficient at a very moderate jet momentum coefficient.[1] There have been several small-scale model tests in wind tunnels at David W. Taylor Naval Ship Research and Development Center to evaluate the characteristics of circulation control airfoils.[2] The application of circulation control aerodynamics to rotor technology is currently being investigated by NASA and the Department of Defense (DOD). With a circulation control rotor, a high thrust is possible at reduced tip speeds and the hub design can be simplified with the elimination of the cyclic pitch.[3,4] Another application of circulation control aerodynamics is on a helicopter tail-boom for producing antitorque forces and replacing the conventional tail rotor altogether (NOTAR).[5] The application of circulation control aerodynamics to the fixed-wing STOL aircraft has also been under consideration.[6]

The object of this paper is to develop an efficient analytical approach to predict the aerodynamic forces on a circulation control elliptical airfoil. In the literature, there have been several efforts to determine experimentally the characteristics of the circulation control airfoils in wind tunnels.[2] But, there have been only a few limited efforts to predict analytically the forces on the circulation control airfoils. For example, Dunham[7] studied analytically the problem of a circular cylinder with a tangential blowing. The wall-jet, as well as the boundary layer, was calculated by an integral method; the

pressure distributions needed for boundary layer calculations were approximated using the experimental data. Due to the complex and rapid changes of wall-jet, the approximate representation of velocity profiles in the integral method becomes quite inaccurate. Dvorak and Kind[8] used an integral method to calculate the boundary layer development and a finite difference method to calculate the wall-jet interaction on a circulation controlled airfoil. They also considered the displacement effects of the boundary layer and the wall-jet on the potential flow calculations. In their method, however, the effects of separated wake were neglected. The separated wake becomes wider with thicker airfoils and, therefore, can play an important role in the pressure calculations through its interaction with the potential flow. In fact, the effect of separated wake must be included for thick sections at moderate levels of blowing. For example, the circulation control tail boom of a helicopter (NOTAR) is nearly a circular airfoil, and hence its wake can be quite wide.

In the present work, the effect of separated wake is included, and it is simulated by distributing source panels on the airfoil surface in the separation region. Using conformal mapping, a very simple and efficient solution procedure is formulated for the potential flow calculations of an elliptical airfoil including the separated wake effects. An iterative procedure is formulated to determine the boundary layer and potential flow interaction effects. The governing equations of the boundary layer and wall-jet are derived in an elliptical coordinate system, so that the effect of surface curvature on laminar flow is automatically introduced. The effect of curvature on the turbulence structure is a complex problem and is not addressed here. A finite difference method is used to solve the governing equations. Combining the potential flow with separated wake calculations and the boundary layer and wall-jet calculations, the flow around a circulation control elliptical airfoil is determined for given blowing jet momentum coefficients and freestream conditions.

Calculation of Potential Flow with Separated Wake Effects

A simple approximation of the surface velocity distribution of an elliptical airfoil is obtained from the potential flow theory[9]

$$\frac{U_e}{U_\infty}=\frac{(1+\lambda)\sin(x_e+\alpha)+(\Gamma/2\pi U_\infty a)}{\{(1-\lambda^2)[\sinh^2(y_{eo})+\sin^2(x_e)]\}^{1/2}} \tag{1}$$

This is perhaps a good approximation for thin elliptical airfoils. For thick elliptical airfoils, the separated wake will become wide and the above relation will be a poor approximation to the surface velocity distribution of the airfoil. Figure 2 shows the comparison of the surface pressure distributions calculated by Eq. (1) and the experimentally determined values[10] for a circular airfoil ($\lambda=1$). Except for a small leading-edge surface, there is a considerable disagreement between these two sets of results.

One simple approach to account for the effects of separated wake is discussed in Ref. 11. In this approach, the sources are distributed on the airfoil surface in the separation region to simulate the displacement effects of the wake (Fig. 3). The strengths of the sources are determined in such a way that the static pressure remains constant on the airfoil surface in the separation region including both the upper and lower separation points. In the present work, this approach is applied to an elliptical airfoil. The formulation is made for a circular airfoil first; then, by the conformal mapping technique, the solution is obtained for elliptical airfoils.

Flow Around a Circular Airfoil

The complex potential function of a circular airfoil in a uniform flow with a circulation Γ is obtained from the sum of the complex potentials corresponding to the uniform flow, the doublet, and the vortex.[9]

$$W_c(Z)=-(U_\infty-iV_\infty)Z-(U_\infty+iV_\infty)(R^2/Z)$$
$$-(i\Gamma/2\pi)\ell n(Z/R) \tag{2}$$

If a source of strength C_s is put on the surface and a sink of strength $C_s/2$ at the center of the circular airfoil (Fig. 4), the complex potential function for this source and sink combination is

$$W_s(z)=(C_s/2\pi)\ell n(Z-Z_0)-(C_s/4\pi)\ell nZ \tag{3}$$

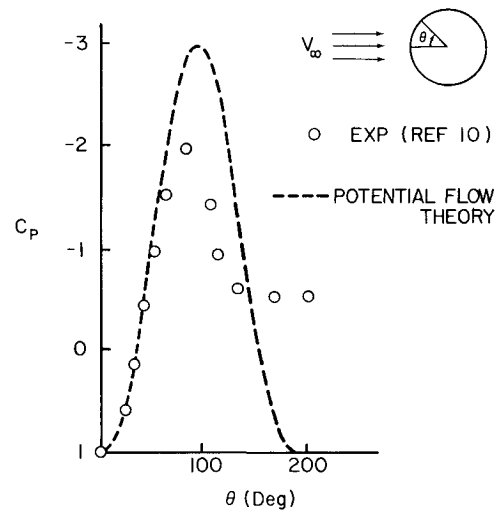

Fig. 2 Pressure distribution on a circular cylinder.

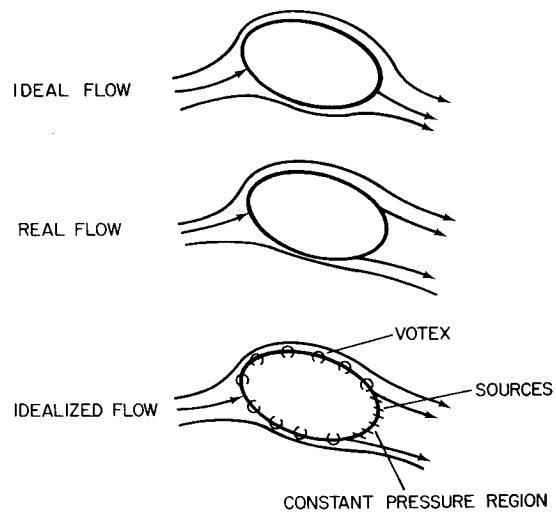

Fig. 3 A sketch of flows around a thick airfoil.

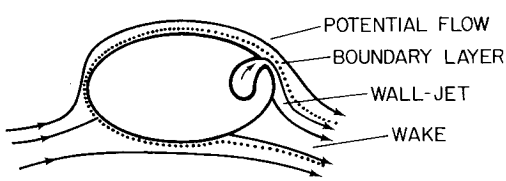

Fig. 1 A circulation control airfoil.

and the velocity potential function of this source and sink combination is

$$\phi_s(x_c,y_c) = (C_s/4\pi)\ell n[(x_c-x_{c_0})^2+(y_c-y_{c_0})^2] - C_s/8\pi)\ell n[x_c^2+y_c^2] \quad (4)$$

The total complex potential function of a circular airfoil in a uniform flow with circulation Γ and with the inclusion of a source and sink combination is given as

$$W(Z) = W_c(Z) + W_s(Z) \quad (5)$$

It can be shown that with this total complex potential, the circle remains a streamline. This is also true when a source panel is put on the surface and a sink with half the total strength of the source panel at the center of the circular airfoil. From Eq. (4), the potential function of the source panel and the sink can be written as

$$\phi_{s_j}(x_c,y_c) = \frac{1}{4\pi}\int_j \ell n[(x_c-x_{c_j})^2+(y_c-y_{c_j})^2]q_j dS_j - \frac{1}{4\pi}\left(\frac{1}{2}\int_j q_j dS_j\right)\ell n(x_c^2+y_c^2) \quad (6)$$

Assuming

$$x_c = R\cos(\theta) \qquad y_c = R\sin(\theta)$$
$$x_{c_j} = R\cos(\theta_j) \qquad y_{c_j} = R\sin(\theta_j)$$
$$q_j = \text{const} \qquad dS = Rd\theta_j$$

The tangential and normal velocities on the surface of the airfoil are obtained from Eq. (6) as

$$U_{\theta_{sj}}(R,\theta) = \frac{q_j}{4\pi}\ell n\frac{1-\cos(\theta-\theta_j)}{1-\cos(\theta-\theta_{j+1})} \quad (7)$$

$$U_{r_{sj}}(R,\theta) = \begin{cases} 0 & \theta<\theta_j, \theta>\theta_{j+1} \\ q_{j/2} & \theta_j<\theta<\theta_{j+1} \end{cases} \quad (8)$$

It is seen that the source panel and sink combination has no contribution to the normal velocity on the surface other than the source panel itself.

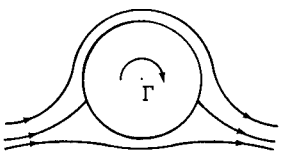

a) STREAMLINES WITH A VORTEX AT THE CENTER

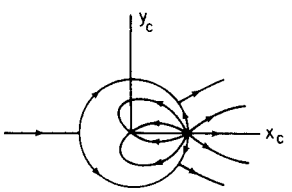

b) STREAMLINES WITH A SOURCE AT THE TRAILING EDGE AND A SINK OF HALF THE STRENGTH AT THE CENTER

Fig. 4 Streamlines of a circular airfoil in uniform flow.

Now, in order to represent the separated wake, N source panels are placed on the circle in the separation region and a corresponding number of sinks at the center of the circle (Fig. 5). The two separation points S_u and S_ℓ are assumed known. The velocity at a point i on the surface of the cylinder consists of the contribution due to the source panels and sinks, the freestream, the vortex, and the doublet. Therefore the tangential and normal velocities at point i are

$$U_\theta(i) = \sum_{j=1}^{N} U_{\theta_{sj}}(R,\theta_j) + U_{\theta_v}(R,\theta_i) + U_{\theta_c}(R,\theta_i) \quad (9)$$

$$U_r(i) = \begin{cases} q_i/2 & \theta_j<\theta_i<\theta_{j+1} \\ 0 & \theta_i>\theta_j \text{ or } \theta_i>\theta_{j+1} \end{cases} \quad (10)$$

where $U_{\theta_{sj}}$ is due to jth source panel and its corresponding sink, the U_{θ_v} is due to the vortex, and the U_{θ_c} is due to the freestream and the doublet. The extreme points of 1 and N,

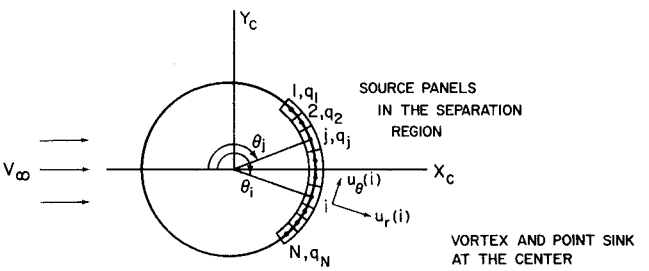

Fig. 5 Complete wake model.

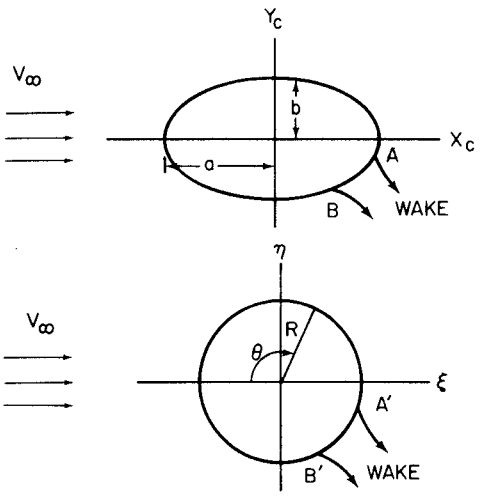

Fig. 6 Transformation from elliptical to circular airfoil.

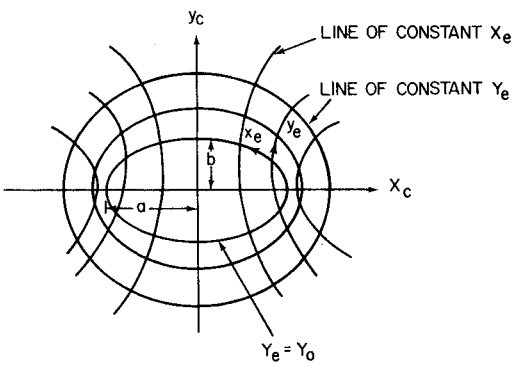

Fig. 7 The elliptical coordinate system.

respectively, correspond to the upper and lower separation points where the normal velocity is zero. Thus,

$$q_1 = q_N = 0 \tag{11}$$

The condition of constant static pressure between points 1 and N requires that

$$\begin{aligned}[U_\theta(i)]^2 + [U_r(i)]^2 &= \text{const} \\ &= [U_\theta(1)]^2 + [U_r(1)]^2 \\ &= [U_\theta(N)]^2 + [U_\theta(N)]^2 \\ i &= 2,3,\ldots(N-1)\end{aligned} \tag{12}$$

Substituting Eqs. (9) and (10) into Eq. (12) gives

$$\left[\sum_{j=2}^{N-1} U_{\theta_{sj}}(R,\theta_i) + U_{\theta_v}(R,\theta_i) + U_{\theta_c}(R,\theta_i)\right]^2 + [U_r(i)]^2 = A \tag{13}$$

$$i = 2,3,\ldots N-1$$

$$\left[\sum_{j=2}^{N-1} U_{\theta_{sj}}(R,\theta_1) + U_{\theta_v}(R,\theta_1) + U_{\theta_c}(R,\theta_1)\right]^2 = A \tag{14}$$

$$\left[\sum_{j=2}^{N-1} U_{\theta_{sj}}(R,\theta_N) + U_{\theta_v}(R,\theta_N) + U_{\theta_c}(R,\theta_N)\right]^2 = A \tag{15}$$

where A is a constant. The velocity term due to vortex can be written as

$$U_{\theta_v}(R,\theta_i) = (\Gamma/2\pi R) \equiv \gamma \tag{16}$$

Substituting Eqs. (7), (8), and (16) into Eqs. (13-15) gives

$$\left[\sum_{j=2}^{N-1} q_j K_{ij} + \gamma + U_{\theta_c}(R,\theta_i)\right]^2 + (q_{i/2})^2 = \left[\sum_{j=2}^{N-1} q_j K_{1j} + \gamma + U_{\theta_c}(R,\theta_1)\right]^2 \qquad i = 2,3,\ldots N \tag{17}$$

where

$$K_{ij} = 1/4\pi \ \ell n[1 - \cos(\theta_i - \theta_j)/1 - \cos(\theta_i - \theta_{j+1})]$$

The $(N-1)$ variables, $q_2, q_3 \ldots, q_{N-1}$ and γ, can be solved from above system of Eqs. (17).

The system of Eqs. (17) are nonlinear algebraic equations. The Newton method is used to solve these equations. Typically, 10 to 15 source panels (of course, depending on the size of the separation region) are used in the calculations, and it is found that more panels will not improve the results significantly. After $q_2, q_3 \ldots q_{N-1}$ and γ are determined, the velocity distribution on the airfoil can be calculated.

Flow Around an Elliptical Airfoil

The flow around an elliptical airfoil can be transformed to that around a circle using the following transformation:

$$Z = \zeta + (\sigma^2/\zeta) \tag{18}$$

where $\sigma = \frac{1}{2}[a^2 - b^2]^{\frac{1}{2}}$ (Fig. 6). Writing $W(Z)$ and $W(\zeta)$ as the complex potential functions in Z-plane and ζ-plane, we have

$$\frac{dW(Z)}{dZ} = \frac{dW(\zeta)}{d\zeta}\ \frac{dZ}{d\zeta} \tag{19}$$

The condition of constant pressure between A and B (Fig. 6) requires that

$$\begin{aligned}[U^2 + V^2]_{\text{between } A \text{ and } B} &= \text{const} \\ &= U_A^2 + V_A^2 \\ &= U_B^2 + V_B^2\end{aligned} \tag{20}$$

From Eq. (19), we have

$$U^2 + V^2 = \left|\frac{dW(Z)}{dZ}\right|^2 = \left|\frac{dW(\zeta)}{d\zeta}\right|^2 \left|\frac{dZ}{d\zeta}\right|^2 = [U'^2 + V'^2]\left|\frac{dZ}{d\zeta}\right|^2 \tag{21}$$

Therefore, the requirement of Eq. (20) is transformed to ζ-plane as

$$\begin{aligned}[U'^2 + V'^2]_{\text{between } A' \text{ and } B'} &= [U'^2_{A'} + V'^2_{A'}]\left|\frac{dZ}{d\zeta}\right|^2_{\text{between } A' \text{ and } B'} \Big/ \left|\frac{dZ}{d\zeta}\right|^2_{A'} \\ &= [U'^2_{B'} + V'^2_{B'}]\left|\frac{dZ}{d\zeta}\right|^2_{\text{between } A' \text{ and } B'} \Big/ \left|\frac{dZ}{d\zeta}\right|^2_{B'}\end{aligned} \tag{22}$$

where

$$\left|\frac{dZ}{d\zeta}\right|^2 = 1 - 2\frac{1-\lambda}{1+\lambda}\cos(2\theta) + \left(\frac{1-\lambda}{1+\lambda}\right)^2$$

If we use Eq. (22) in place of Eq. (12) and proceed in the same way as in the treatment of the circle, the circulation and the stengths of source panels and sinks can be determined for the elliptical airfoil.

The input data required here are the positions of the separation points, freestream velocity, the airfoil geometry, and the angle of attack.

Calculations of Boundary Layers and Wall-Jet

Governing Equations

The governing equations of the boundary layer and wall-jet are derived in an elliptical coordinate system (Fig. 7), so that the effects of the surface curvature can be automatically introduced. The equations are as follows.

Continuity equation:

$$\frac{1}{h_1}\frac{\partial U}{\partial x_e} + \frac{1}{h_2}\frac{\partial V}{\partial y_e} + \frac{1}{h_1 h_2}\frac{\partial h_2}{\partial x_e}U + \frac{1}{h_1 h_2}\frac{\partial h_1}{\partial y_e}V = 0 \tag{23}$$

Momentum equation x-direction:

$$\begin{aligned}&\frac{U}{h_1}\frac{\partial U}{\partial x_e} + \frac{V}{h_2}\frac{\partial U}{\partial y_e} + \frac{1}{h_1 h_2}\frac{\partial h_1}{\partial y_e}UV + \frac{1}{h_1}\frac{\partial}{\partial x_e}\left(\frac{P}{\rho}\right) \\ &+ \frac{1}{h_2}\frac{\partial}{\partial y_e}\overline{U'V'} + 2\frac{1}{h_1 h_2}\frac{\partial h_1}{\partial y_e}\overline{U'V'} \\ &- \nu\left\{\frac{1}{h_1 h_2}\frac{\partial}{\partial y_e}\left(\frac{h_1}{h_2}\frac{\partial U}{\partial y_e}\right)\right. \\ &- 2\frac{1}{h_1 h_2}\frac{\partial h_2}{\partial x_e}\frac{\partial V}{\partial y_e} - \left[\left(\frac{1}{h_1 h_2}\frac{\partial h_1}{\partial y_e}\right)^2\right. \\ &\left.\left. + \left(\frac{1}{h_1 h_2}\frac{\partial h_2}{\partial x_e}\right)^2\right]U\right\} = 0\end{aligned} \tag{24}$$

Momentum equation y-direction:

$$-\left(\frac{1}{h_1 h_2}\frac{\partial h_1}{\partial y_e}\right)U^2+\frac{1}{h_2}\frac{\partial}{\partial y_e}\left(\frac{P}{\rho}\right)=0 \qquad (25)$$

The boundary conditions at the surface are

$$U(x_e,y_{e_0})=0 \qquad V(x_e,y_{e_0})=0$$

and at the edge of the boundary layer

$$U(x_e,y_{e_\infty})=U_e(x_e) \qquad P(x_e,y_{e_\infty})=P_e(x_e) \qquad (26)$$

The relationships between elliptical coordinates and Cartesian coordinates are

$$x_c=\ell\cosh(y_e)\cos(x_e)$$
$$y_c=\ell\sinh(y_e)\sin(x_e) \qquad (27)$$

where $\ell=(a^2-b^2)^{1/2}$. From Eq. (27), it can be shown that

$$h_1=h_2=\ell[\sinh^2(y_e)+\sin^2(x_e)]^{1/2}\equiv h \qquad (28)$$

The y_e-coordinate line that coincides with the elliptical airfoil surface is determined by

$$e^{y_{eo}}=[(a+b)/(a-b)]^{1/2} \qquad (29)$$

Reynolds' Stress Modeling

In order to solve Eqs. (23-25), it is necessary to relate the Reynolds' stress to the mean velocity distribution. The eddy-viscosity model for the turbulent boundary layer used here is due to Cebeci and Smith.[12] The Reynolds' stress model for the wall-jet, superposed by the upstream turbulent boundary layer, is taken from Dvorak.[13]

Solution Procedure

For solving the system of Eqs. (23-25), it is convenient to introduce the new independent variables to stretch the boundary layer thickness. The following coordinate transformation is introduced

$$\tilde{x}=x_e \qquad d\tilde{y}=\left[\frac{U_e(x_e)}{\upsilon L(x_e)}\right]^{1/2}h\,dy_e \qquad (30)$$

where

$$L=\int_{x_{e_0}}^{x_e}h(x_e,y_{e_0})dx_e$$

A stream function, $\psi(x_e,y_e)$, is introduced to satisfy the continuity equation and is defined as

$$-\frac{1}{h}\frac{\partial\psi}{\partial x_e}=V \qquad \frac{1}{h}\frac{\partial\psi}{\partial y_e}=U \qquad (31)$$

and its dimensionless form, $f(\tilde{x},\tilde{y})$, is given by

$$\psi(x_e,y_e)=(U_e\upsilon L)^{1/2}f(\tilde{x},\tilde{y}) \qquad (32)$$

Rewriting Eqs. (23-25) we have

$$C_1 f'''=C_2 f''+C_3 f'+[C_4 f'-C_5 f'']\frac{\partial}{\partial\tilde{y}}\left(\frac{\epsilon}{h\upsilon}\right)+C_6\bar{P}$$
$$+C_7 f'^2+C_8 f f''+C_9\left(f'\frac{\partial f'}{\partial\tilde{x}}-f''\frac{\partial f}{\partial\tilde{x}}\right)+C_{10}\frac{\partial\bar{P}}{\partial\tilde{x}} \qquad (33)$$

$$\frac{\partial\bar{P}}{\partial\tilde{y}}=C_{11}f'^2 \qquad (34)$$

The boundary conditions are

$$f(\tilde{x},\tilde{y}_0)=0 \qquad f'(\tilde{x},\tilde{y}_0)=0$$

$$\lim_{y\to\infty}\frac{h(\tilde{x},\tilde{y}_0)}{h(x,y)}f'(\tilde{x},\tilde{y})=1 \qquad \lim_{y\to\infty}\bar{P}(\tilde{x},\tilde{y})=\bar{P}_e(\tilde{x}) \qquad (35)$$

where

$$(\,)'=\frac{\partial}{\partial\tilde{y}}(\,) \qquad \bar{P}=\frac{P-P_0}{\rho U_e^2}$$

$$C_1=1+\frac{\epsilon}{\upsilon} \qquad C_2=\frac{2}{h}\frac{\partial h}{\partial\tilde{y}}$$

$$C_3=\frac{1}{h}\frac{\partial^2 h}{\partial\tilde{y}^2}-\frac{1}{h^2}\left(\frac{\partial h}{\partial\tilde{y}}\right)^2+\left(\frac{\epsilon}{h\upsilon}\right)\frac{\partial^2 h}{\partial\tilde{y}^2}$$
$$+\frac{1}{h_2\beta^2}\left[\frac{\partial h}{\partial\tilde{x}}+\frac{\partial h}{\partial\tilde{y}}\frac{\partial\tilde{y}}{\partial x_e}\right]^2$$

$$\beta=\left(\frac{U_e}{\upsilon L}\right)^{1/2} \qquad C_4=\frac{\partial h}{\partial\tilde{y}}$$

$$C_5=h \qquad C_6=\frac{2L}{U_e h_0}\frac{\partial U_e}{\partial\tilde{x}}\left(\frac{h}{h_0}\right)^2 \qquad (h_0=h(\tilde{x},\tilde{y}_0))$$

$$C_7=\frac{L}{h_0 U_e}\frac{\partial U_e}{\partial\tilde{x}}+\frac{L}{h_0}\left(\frac{1}{h_0}\frac{\partial h_0}{\partial\tilde{x}}-\frac{1}{h}\frac{\partial h}{\partial\tilde{x}}\right)$$

$$C_8=-\frac{1}{2}\left(1+\frac{1}{U_e}\frac{1}{h_0}\frac{\partial U_e}{\partial\tilde{x}}\right) \qquad C_9=\frac{L}{h_0}$$

$$C_{10}=\frac{Lh^2}{h_0^3} \qquad C_{11}=\frac{h_0^2}{h^3}\frac{\partial h}{\partial\tilde{y}}$$

Keller-Cebeci's finite difference method[14] is used to solve Eqs. (33-35). The boundary layer calculation starts from the forward stagnation point. Heimenz's stagnation flow solution[15] gives the initial velocity profile. For some cases, the pressure gradient near the leading edge of the airfoil is sufficiently adverse to cause laminar boundary layer separation. In general, the flow will become turbulent and reattach as a turbulent boundary layer. An empirical criterion formed in Ref. 16 is used to detect transition condition and also to predict the reattachment condition of the flow. It is to be noted that the experiment data used for comparison has specified transition portions since the wire-tapping near leading edge was employed. However, for correlation studies, the transition positions are specified in the experiment (because of wire-tapping) and these are used for calculations.

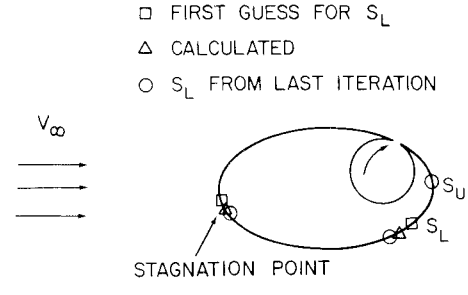

Fig. 8 A sketch illustrating the calculation process.

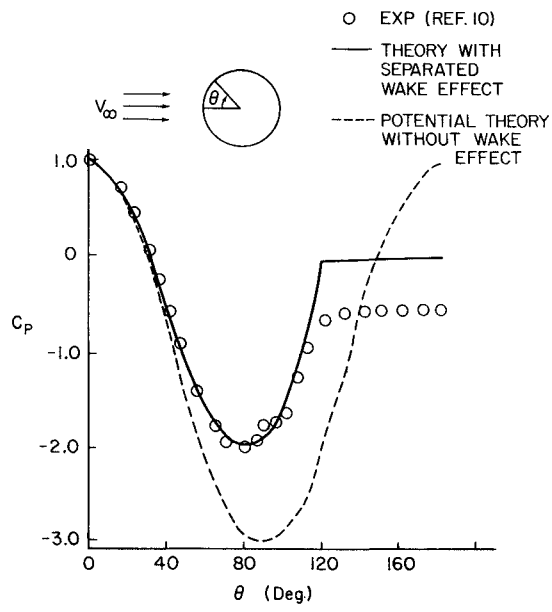

Fig. 9 Pressure distribution on a circular cylinder, Reynolds number = 1.08×10^5.

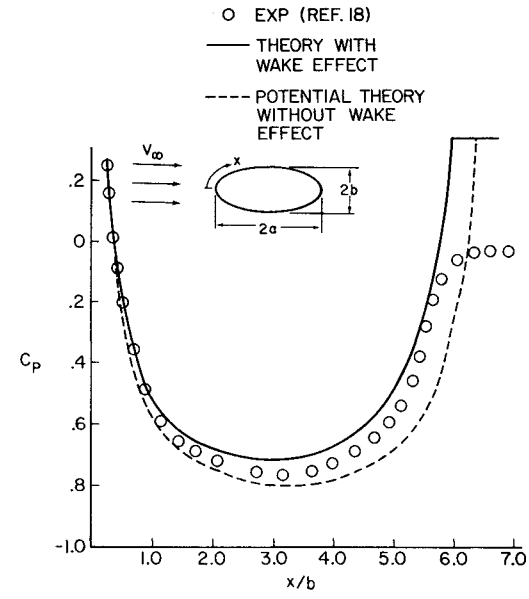

Fig. 10 Pressure distribution on an elliptical cylinder with laminar separation, $b/a = 0.3$, Reynolds number = 76,500.

Combined Flows

Combining the potential flow with separated wake effect calculations and boundary layer and wall-jet calculations, the momentum of the blowing jet required to produce a specified lift for the prescribed flight condition can be calculated. Since the potential flow and boundary layer flow interact with each other, an iterative process is adopted. The calculation process is as follows:

1) First the separation point of the upper boundary layer S_U (Fig. 8) is prescribed.

2) Then guess at a separation point for the lower boundary layer S_L, and, with the S_U and S_L, the potential flow with separated wake effect is calculated.

3) With the results from 2, the development of lower boundary layer is calculated. A new separation point is obtained, denoted as S_L'.

4) If S_L is significantly different from S_L, S_L is replaced by S_L' and steps 2-4 are repeated. The above process is continued until S_L is not significantly different from the previous one.

5) We calculate the development of the upper boundary layer with the blowing jet and then keep adjusting the jet momentum until the upper boundary layer separates at S_U.

If the wake is neglected in the potential flow calculations, the iteration process given by Dunham[7] is followed.

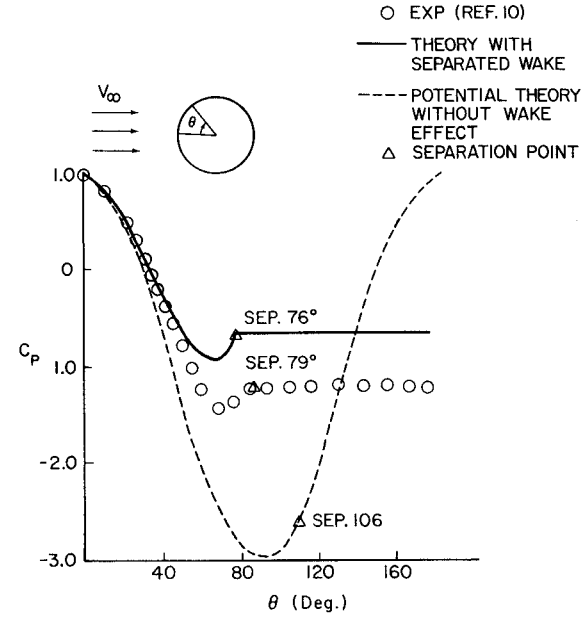

Fig. 11 Pressure distribution on circular cylinder with laminar separation, Reynolds number = 1.08×10^5.

Results and Discussion

The calculation method has been applied to some selected circulation control airfoils. First the potential flow results including the separated wake effects are presented. The calculated and measured pressure distributions are shown for a cylinder as well as an elliptic airfoil with thickness ratio of 0.3 in Figs. 9 and 10, respectively, for no blowing conditions. For these calculations, the separation points are taken from the experimental data.[10,18] It is seen that a good agreement between the calculated and the measured pressure distributions before the separation point is obtained. However, there are discrepancies between the theory and experiment near and after the separation point. This discrepancy is perhaps due to the simplified modeling of the separated wake.

In general, the separation points are not known and these have to be determined by an iterative procedure combining viscous and potential flows. Figure 11 shows the comparison between the measured and the calculated separation points of a laminar boundary layer and the pressure distributions for a circular airfoil with zero circulation (no blowing). In the calculations, the pressure distribution from the potential theory without the wake effect is used to obtain the first estimate of the separation points. These first calculated separation points are then used in the potential flow calculations including the separated wake effects to obtain a new pressure distribution which in turn is used in the boundary layer calculations to obtain the improved separation points, and henceforth. This iteration process is carried on until the calculated separation point is not significantly different from the previous one. From Fig. 11, the boundary layer calculation with pressure distribution from potential theory without wake effect predicts separation at $\phi = 106$ deg; the iteration between potential flow with separated wake effect calculation and boundary layer calculation predicts separation at $\phi = 76$ deg, which is only 3 deg different from the measured value of $\phi = 79$ deg.[10] This small discrepancy in the prediction of the

separation point is believed to be caused by the inaccurate pressure calculation near the separation point (see Fig. 9). The similar type of calculations were carried out for a circular airfoil with the turbulent boundary layer separation and the results are compared with the experimental data[17] in Fig. 12. Again, the predicted separation point is quite close to the measured one. Figure 13 shows the comparison between the calculated and the measured pressure distributions and the separation points for an elliptical airfoil of 30% thickness ratio for no blowing condition. In this case, the iteration between the potential flow with separation wake effect calculation and boundary layer calculation predicts the separation point at a station which is much earlier than that measured by the experiment.[18] From the results in Figs. 11-13, it can be said that the combination of the potential flow with separated wake effect calculations and the boundary layer calculations can predict the separation point reasonably well for very thick airfoils, but it predicts separation too early for thinner airfoils.

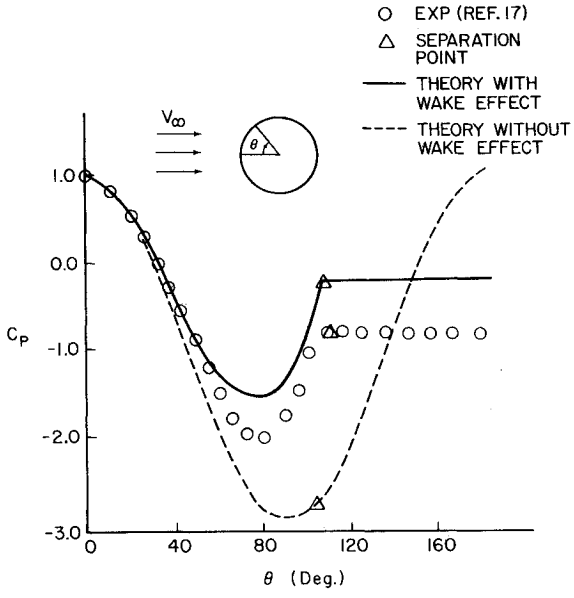

Fig. 12 Pressure distribution on circular cylinder with turbulent separation, Reynolds number = 5.01×10^5.

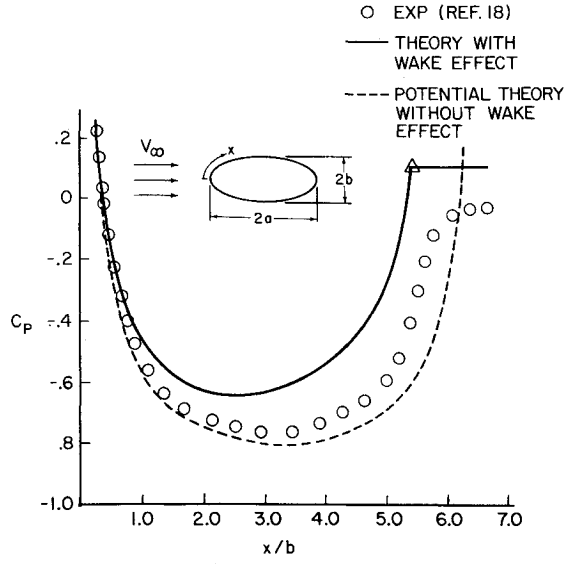

Fig. 13 Pressure distribution on elliptical cylinder with turbulent separation, $b/a = 0.3$, Reynolds number = 139,000.

Further calculations were made for circular and elliptical airfoils with blowing. Figure 14 shows the calculated lift coefficients for a range of jet momentum coefficient, with and without the inclusion of wake effects. A very significant effect of the separated wake on the calculated results is seen. We do not have experimental data for this case.

Figure 15 shows the calculated lift coefficient with the varying jet momentum coefficient for an elliptical airfoil of 20% thickness ratio. The experimental results from Ref. 1 are also presented. The calculated results with wake effect do not agree with experimental data; this is because, with thin airfoils, the iteration between potential flow with separated wake effect calculation and boundary layer calculation does not predict separation correctly. Calculations neglecting the wake effect were made and results are also shown in Fig. 15. The calculated results neglecting the wake effect agree with the experiment at low- and moderate-momentum coefficients. At high-momentum coefficients, the lift coefficient is underestimated. The discrepancy between calculated and experimental results increases with jet momentum coefficient. This discrepancy is not due to the wake effect since the wake becomes narrower as circulation around the airfoil increases. One factor contributing to the discrepancy may be the importance of the entrainment effect of the jet on the potential flow. This effect increases with the jet momentum. The simple turbulence model for the wall-jet used in the present analysis may be another factor causing the above discrepancy. Improvement on these aspects is needed in the future work. Additional calculations neglecting the separated wake for the above elliptical airfoil at different angles of attack are shown in Fig. 16. The results are similar to that in Fig. 15.

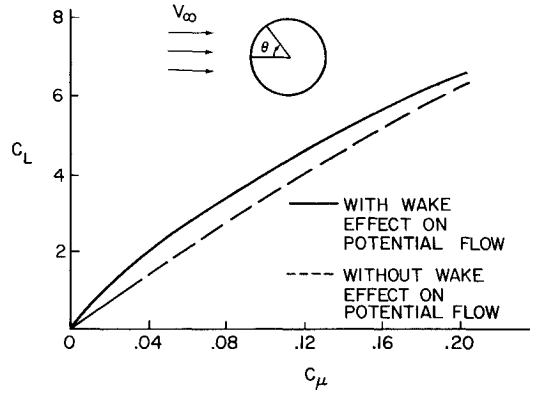

Fig. 14 Lift coefficient vs momentum coefficient for circular cylinder, Reynolds number = 1.85×10^5, $\theta_{jet} = 105$ deg.

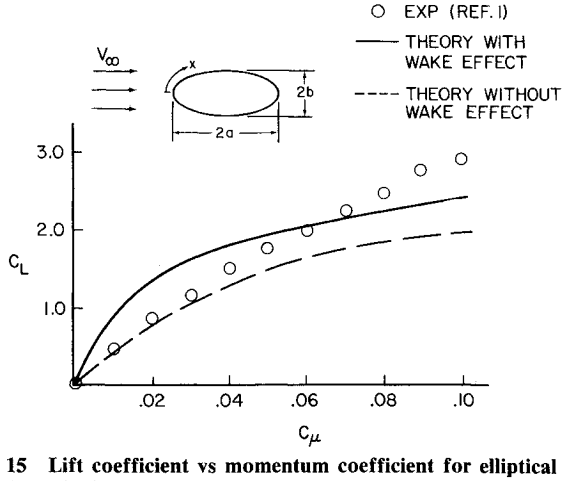

Fig. 15 Lift coefficient vs momentum coefficient for elliptical airfoil, $b/a = 0.23$.

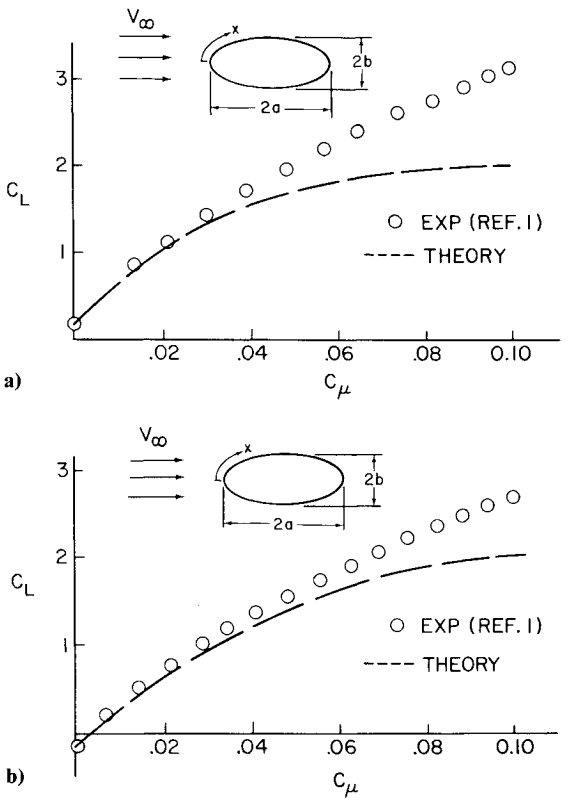

Fig. 16 Lift coefficient vs momentum coefficient for elliptical airfoil, Reynolds number $= 7.5 \times 10^5$, $x_{jet}/2a = 1.0025$; a) angle of attack = 2 deg; b) angle of attack = −2 deg.

Conclusions

A simple solution is obtained to the potential flow with separated wake effect for elliptical airfoils. When combined with boundary layer theory, it gives good results for pressure distribution and separation position for thick airfoils, but the results become less satisfactory as the thickness ratio of the airfoil decreases. The separated wake has significant effects on the calculation of aerodynamic forces on a circulation control airfoil of large thickness ratio. For thin airfoils, the separated wake can be neglected. Future work should include entrainment effect of the wall-jet on the potential flow.

Acknowledgments

The authors acknowledge with appreciation the assistance of Mr. Raghavan. The work was partially supported by the David W. Taylor Naval Ship Research Development Center under Contract N00167-85-C-0077. The Technical monitor was Dr. T. C. Tai.

References

[1]Kind, R. J. and Maull, D., "An Experimental Investigation of a Low-Speed Circulation Controlled Airfoil," *Aeronautical Quarterly*, Vol. 19, May 1968, pp. 170-182.

[2]Englar, R. J. and Applegate, C. A., "Circulation Control—A Bibliography of DTNSRDC Research and Selected Outside References," David W. Taylor Research and Development Center, Bethesda, MD, Rept. DTNSRDC-84/052, Sept. 1984.

[3]Cheeseman, I. C., "The Application of Circulation-Control by Blowing to Helicopters," *Journal of the Royal Aeronautical Society*, Vol. 71, July 1967, pp. 451-467.

[4]Reader, K. R., Kirkpatric, D. G., and Williams, R. M., "Status Report on Advanced Development Program Utilizing Circulation Control Rotor Technology," Presented at Fourth European Rotorcraft and Powered Lift Aircraft Forum, Stresa, Italy, Sept. 1978.

[5]Logan, A. H., "Evaluation of a Circulation Control Tail Boom for Yaw Control," USARTL TR-78-10, 1978.

[6]Englar, R. F., Trobaugh, L. A., and Hemmerly, R. A., "STOL Potential of the Circulation-Control Wing for High Performance Aircraft," *Journal of Aircraft,* Vol. 15, March 1978, pp. 175-181.

[7]Dunham, J., "A Theory of Circulation Control by Slot-Blowing, Applied to a Circular Cylinder," *Journal of Fluid Mechanics,* Vol. 33, Part 3, Sept. 1968, pp. 495-514.

[8]Dvorak, F. A. and Kind, R. J., "Analysis Method for Viscous Flow Over Circulation Control Airfoils," *Journal of Aircraft*, Vol. 16, Jan. 1979, pp. 23-28.

[9]Batchelor, G. B., *An Introduction to Fluid Dynamics*, Cambridge University Press, London, 1970.

[10]Fage, A. and Falkner, V. M., "Further Experiments on the Flow Around a Circular Cylinder," ARC R & M 1369, 1931.

[11]Geller, W., "Calculation of the Turning Angle of Two-Dimensional Incompressible Cascade Flow," *AIAA Journal*, Vol. 14, March 1976, pp. 297-298.

[12]Cebeci, T. and Smith, A.M.O., "Analysis of Turbulent Boundary Layers," Academic Press, New York, 1974.

[13]Dvorak, F. A., "Calculation of Turbulent Boundary Layer and Wall-Jet Over Curved Surfaces," *AIAA Journal*, Vol. 11, April 1973, pp. 517-524.

[14]Keller, H. B. and Cebeci, T., "Accurate Numerical Methods for Boundary Layer Flows II, Two-Dimensional Turbulent Flows," *AIAA Journal*, Vol. 10, Sept. 1972, p. 1193-1199.

[15]Schlichting, H., *Boundary Layer Theory,* 7th ed., McGraw-Hill Book Co., New York, 1979.

[16]Dvorak, F. A. and Woodard, F. A., "A Viscous/Potential Flow Interaction Method for Multi-Element Infinite Swept Wings," NASA CR-2476, Nov. 1974.

[17]Patel, V. C., "The Effect of Curvature on the Turbulent Boundary Layer," ARC R&M 3599, Aug. 1968.

[18]Schubauer, G. B., "Air Flow in the Boundary Layer of an Elliptical Cylinder," NACA Rept. 652, 1939.